ANALYSIS OF A PERMANENT MAGNET DC MOTOR EXPLOSION-REMOVAL ROBOT SYSTEM BASED ON THERMAL ENERGY OPTIMIZATION CONTROL

by

Xingzhi HU [a,b*]

[a] School of Mechanical and Electrical Engineering,
North China Institute of Science and Technology, Beijing, China
[b] Hebei Key Laboratory of Safety Monitoring of Mining Equipment, Langfang, China

Original scientific paper
https://doi.org/10.2298/TSCI2104991H

Based on the quasi-limit theory's design principle, the paper analyzes the steady-state and transient temperature rise laws of the motor with different overload currents from the heat transfer perspective of permanent magnet DC motors. The paper takes the EOD robot as an example. Using this law, the current overload, and temperature rise of the robot wheel motor is analyzed. The study found that the continuous-duty motor (S1) selected is conservative and has an extensive design margin.

Key words: *permanent magnet, DC motor, thermal analysis, overload, temperature rise test, heat transfer calculation, robot*

Introduction

The EOD robot's design life is long, but the total working time during service is 200-300 hours. Based on years of experience in superior robot design, the author established a quasi-limit design theory. The principle is to make the theoretical calculation limit of the equipment as close to the actual limit as possible to analyze high power permanent magnet motors, scholars generally use the finite element method. To analyze low power permanent magnet motors, lumped analysis is used, that is, the motor is regarded as a whole for thermal analysis. Using finite element analysis, you can describe the temperature rise of each part of the motor accurately. However, this method is very cumbersome to model and cannot be entirely suitable for the variable motor load on the robot, and the lumped analysis method is too simplified and not suitable for the actual life estimation of the motor [1].

This paper analyzes the factors that affect the life of permanent magnet DC motors. Under both steady-state and transient conditions, the heat transfer and temperature rise of permanent magnet DC motors are theoretically analyzed. On this basis, the wheel of the EOD robot is analyzed. The electric motor is selected, and the steady-state and transient temperature rise of the wheel motor under the overload current is obtained. The experiment proves that the wheel motor can work safely and reliably. There are 14 permanent magnet DC motors on the EOD robot, which are also equipped with 14 reducers. Through quasi-limit design theory, the total weight is reduced to 20 kg, which improves the robot's flexibility.

* Author's e-mail: 895757507@qq.com

Factors affecting the overload capacity of permanent magnet DC motors

The influence of insulating material on the overload capacity of the motor

Tests have proved that the continuous operating life of the insulating material at the rated temperature θ_N is approximately 6-8a (the average can be 7a). Therefore, insulation life at different operating temperatures can be expressed:

$$D = 7 \times 2^{(\theta_N - T)/m} \tag{1}$$

where m is a constant, for B, F, and H class insulation, take 10, 12, and 14, respectively, for the provisions of θ_N, see the national standard GB-755-87.

The influence of the electric spark between the brush and the commutator on the overload capacity

The commutation problem of permanent magnet motors is very complicated. Poor commutation will produce electric sparks between the brush and the commutator. When the electric spark is large enough, it may damage the brush and commutator surface, which will cause the motor. The torque cannot be output usually. The permanent magnet DC motor's total working time on the EOD robot is only 200-300 hours, so electric sparks' requirements should be wider than the national standard. The differences in each motor manufacturer's technology and materials can be used in specific applications by on-site testing and inquiring about the manufacturer [2].

The influence of the material of the permanent magnet pole on the overload capacity

Rare earth permanent magnet motors have the characteristics of small size, high efficiency, and massive torque. Therefore, this type of motor is widely used in unique robots. The permanent magnet of the motor on the EOD robot has a shallow Curie point. The motivation manufacturer stipulates: it should not exceed 100 °C, otherwise irreversible demagnetization may occur. The magnetic poles are usually installed on the motor housing, so the motor housing's maximum temperature in practical applications is 100 °C.

Temperature rise and heat transfer model under overload current

Most of the EOD robots use enclosed permanent magnet DC motors. Using lumped analysis, the motor is divided into three parts: the armature, the end cover of the motor housing, and the cylindrical housing. It is assumed that:

– the armature material is uniform because the copper heat capacity is relatively close to the heat capacity of the iron core,
– all the heat generated by the motor comes from the armature, and
– it is assumed that the temperature of the air gap between the armature of the motor and the casing is the same at any time [3].

Basic heat conduction and convection heat transfer equation

The presence of a temperature gradient in a uniform object will cause energy transfer inside the air gap, and the transfer rate can be expressed:

$$q = -kA\frac{\partial T}{\partial_x} \tag{2}$$

where k is the thermal conductivity and θ_∞ – the heat transfer area of the conductor. If the upstream temperature of the fluid is A, the concrete surface temperature is θ_s, and h is the convective heat transfer coefficient, the heat transfer rate can be calculated by Newton's law of cooling:

$$q = hA(\theta_s - \theta_\infty) \tag{3}$$

Heat transfer model of steady-state temperature rise under overload current

Analysis of armature heat conduction

Assuming that the armature's temperature rise is symmetrical about the axial centerline of the armature, the cross-section through the axial centerline of the armature can be regarded as an insulating surface in fig. 1.

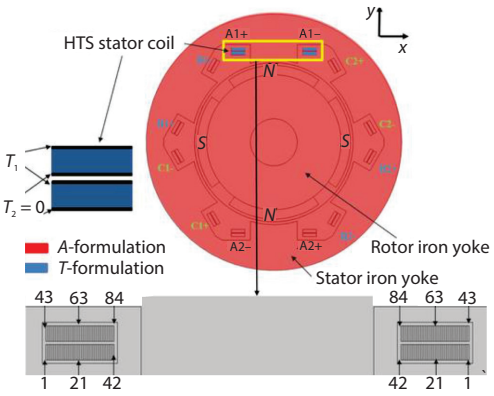

Figure 1. Armature heat transfer model

In the figure θ_g is the air temperature in the air gap, L_a – the length of the armature, and D_a – the outer diameter of the armature. On the armature, we take a micro-element with a thickness of dx and apply the First law of thermodynamics, obtained in a steady-state eq. (4). The newly generated energy on the energy + dx was introduced at x the energy conducted at x + dx the convectively transmitted energy. The article makes $\Delta\theta_1 = \theta_1 - \theta_g$ and $n_1 = 4\bar{h}/kD_a$. Where h is the heat transfer coefficient of forced convection in the motor:

$$\frac{\mathrm{d}^2\Delta\theta_1}{\mathrm{d}x^2} - n_1^2\Delta\theta_1 = -\frac{4p'}{kD_a} \tag{4}$$

where p' is the heating power per unit area of the armature surface and $p' = P_h/(\pi D_a L_a)$, P_h – the healing power of the motor. Solve the eq. (4), and substitute the boundary condition $\mathrm{d}\theta_1/\mathrm{d}x|_{x=0}$ into:

$$\theta_1 = C_1\left(e^n r^x + e^{-n_1 x}\right) + \frac{p'}{h} + \theta_g \tag{5}$$

Heat conduction of motor housing

Our analysis is the same as the previous analysis of the armature. Assuming that the motor housing's temperature rise is symmetrical about the axial centerline, the cross-section through the housing's axial centerline can be regarded as an insulating surface, as shown in fig. 2. For modelling convenience, Divide the motor housing into two parts: the end cover and the cylindrical part.

The end covers Part. Take the ring with width dr on the end cover as the micro-element, according to eq. (4), set the thickness of the end cover as t, and the natural-convection heat transfer coefficient of the motor end cover as $\overline{hV}$, and establish the equation:

$$\frac{\mathrm{d}^2\theta_2}{\mathrm{d}r^2} + \frac{1}{r}\frac{\mathrm{d}\theta_2}{\mathrm{d}r} - n_2^2\theta_2 = 0 \tag{6}$$

where

$$\theta_2 = t_2 - \frac{\bar{h}\theta_g + \bar{h}V\theta_\infty}{\bar{h} + \bar{h}V}, \quad n^2 = \frac{\overline{\bar{h} + \bar{h}V}}{kt}$$

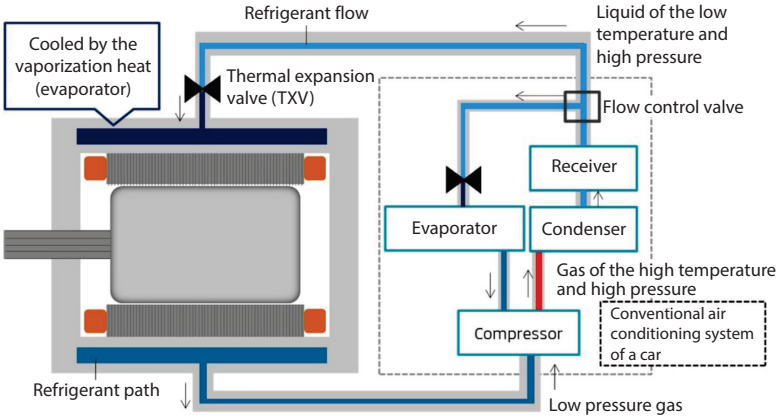

Figure 2. Heat transfer model of the motor shell

Equation (6) is the zero-order Bessel differential equation, and its general solution:

$$\theta_2 = C_3 I_0(n2r) + C_4 K_0(n_2 r) \tag{7}$$

where I_0 is the first kind of zero-order modified Bezier function and K_0 – the second kind of zero-order modified Bezier function [4].

Cylinder Part. As shown in fig. 2, the wall thickness and the end cover thickness are the same as t, and a ring with width dx is taken as a micro-element on the cylinder. The natural-convection heat transfer coefficient of the cylindrical motor shell is $\overline{hc}$ we build the equation:

$$\frac{\mathrm{d}^2 \Delta\theta_3}{\mathrm{d}x^2} - n_3^2 \Delta\theta_3 = 0 \tag{8}$$

where

$$\Delta\theta_3 = \theta_3 - \frac{\overline{h}(a-t)\theta_g + \overline{h}ca\theta_\infty}{\overline{h}(a-t) + \overline{h}ca\theta_\infty}, \quad n^3 = \frac{2\left[\overline{h}(a-t) + \overline{h}ca\right]}{kt(2a-t)}$$

Solve eq. (8) and substitute boundary condition $\mathrm{d}\theta_3/\mathrm{d}x|_{x=Lj/2}$ to obtain:

$$\Delta\theta_3 = C_5\left[e^{n_3 x} + e^{n_3(L_j - x)}\right] \tag{9}$$

where in eqs. (5), (7), and (9), there are five unknowns: C_1, θ_g, C_3, C_4, and C_5, under steady-state conditions, θ_g can be approximated as the average temperature of the entire motor, and the other four unknown parameters need to be determined. According to the four boundary conditions, the following four equations can be obtained:

$$\begin{gathered}
\theta_1\left(\frac{L_a}{2}\right) = \theta_2(b) \\
\theta_2(a) = \theta_3(0) \\
-k\frac{1}{4^\pi} b_2 \theta_1'(x) + \int_b^a 2\pi r\overline{h}\left[\theta_g - \theta_2(x)\right]\mathrm{d}r + \int_0^{L_j/2} 2\pi(a-t)\overline{h}\left[\theta_g - \theta_3(x)\right]\mathrm{d}r = \\
= \frac{P_h}{2} - k2\pi b\theta_2'(x) + \frac{1}{4}\pi b^2 \overline{h}_V\left[\theta_1\left(\frac{L_a}{2}\right) - \theta_\infty\right] = -k\frac{1}{4}\pi b^2 \theta_1'(x)
\end{gathered} \tag{10}$$

Once these four unknowns' values are determined, the temperature rise law of the permanent magnet DC motor at a given armature current is also determined [5].

Transient temperature rise heat transfer model under overload current

Simplification of the natural-convection heat transfer coefficient of the motor surface

To facilitate the analysis, the natural-convection heat transfer coefficient of the motor surface is simplified, and the original curve is replaced by a straight line at 50 °C and 100 °C, see straight line 1 in fig. 3. Similarly, the motor housing's cylindrical surface can also be the natural-convection heat transfer coefficient is linearized:

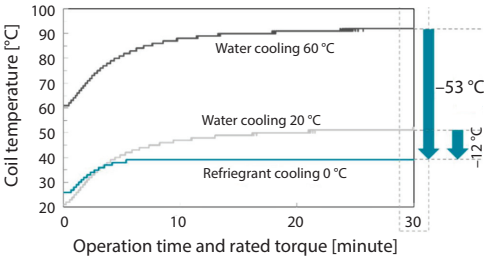

Figure 3. The change of natural-convection heat transfer coefficient with end cover temperature

$$\overline{h}_V = k_V(\theta_j - 50) + \overline{h}_{V50}$$
$$\overline{h}_V = k_C(\theta_j - 50) + \overline{h}_{V50}$$

where θ_j is the temperature of the motor casing, $k_V = (\overline{h}_{V100} - \overline{h}_{V50})/50$, $\overline{h}_{V50}$, and $\overline{h}_{V100}$ are the average natural-convection heat transfer coefficients of and at the end cover of the motor casing, respectively, $k_c = (\overline{h}_{C100} - \overline{h}_{C50})/50$, $\overline{h}_{C50}$, and $\overline{h}_{C100}$ are the average natural-convection heat transfer coefficients of the cylindrical surface of the motor casing and, respectively [6].

Determination of the transient temperature rise of the motor

According to the law of conservation of energy, it is known that the total heat generated by the motor = the increase in the internal energy of the motor + the heat emitted by the motor [7]:

$$-mc\mathrm{d}\theta_j = [\theta_j^2 - (\theta_{m4} + \theta_\infty)\theta_j - (\theta_{m4}\theta_\infty + P_{h1})]\mathrm{d}t$$
$$\theta_{m4} = -\frac{-100L_j kc + 2L_j\overline{h}_{C50} - 50D_j k_V + D_j\overline{h}_{V50}}{2L_j kc + D_j k_V} \tag{11}$$

where

$$k_f = \frac{1}{2}\pi D_j(2L_j kc + D_j k_V),\ mc = m\frac{C_p}{k_f},\ P_{h1} = \frac{P_h}{k_f}$$

Solve the differential eq. (11), we can get:

$$\theta_j = \frac{\theta_5 - C_1\theta_4\exp\left(-\dfrac{2\theta_{m5}}{mc}t\right)}{1 + C_1\exp\left(-\dfrac{2\theta_{m5}}{mc}t\right)},\ \theta_{m5}^2 = P_{h1} + \frac{1}{4}(\theta_{m4} - \theta_\infty)^2 \tag{12}$$

where

$$\theta_4 = -\frac{1}{2}(\theta_{m4} + \theta_\infty) + \theta_{m5},\ \theta_5 = \frac{1}{2}(\theta_{m4} + \theta_\infty) + \theta_{m5},\ C_1 = \frac{\theta_5 - \theta_m}{\theta_4 + \theta_m}\theta_m$$

is the starting temperature of the permanent magnet DC motor. Equation (12) applies to the motor shell range 50 °C $\leq \theta_j \leq$ 100 °C. If the temperature of the motor casing is known, the time

taken by the motor from the initial temperature to the current temperature can be approximated according to eq. (12):

$$t_1 = \frac{mc}{2\theta_{m5}} 1n \frac{(\theta_5 - \theta_m)(\theta_j + \theta_4)}{(\theta_4 + \theta_m)(\theta_5 - \theta_j)} \tag{13}$$

Load analysis and test

The EOD robot, see fig. 4 is mainly in the urban environment and buildings, which can generally be divided into flat ground, slopes, and stairs. The load analysis shows that the maximum torque required for the robot to go up the stairs is required for flat ground. More than 10 times the torque is more than two times the maximum slope torque, so it can be approximated that the load on the flat ground will not affect the wheel motor's life, as long as the two working environments of slope and stairs are considered [8].

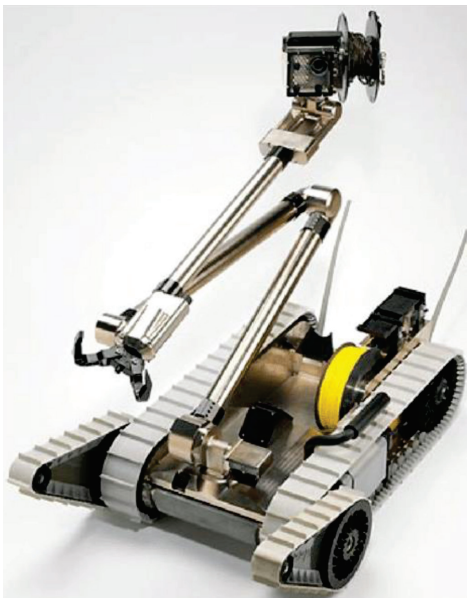

Figure 4. Entity diagram of EOD robot

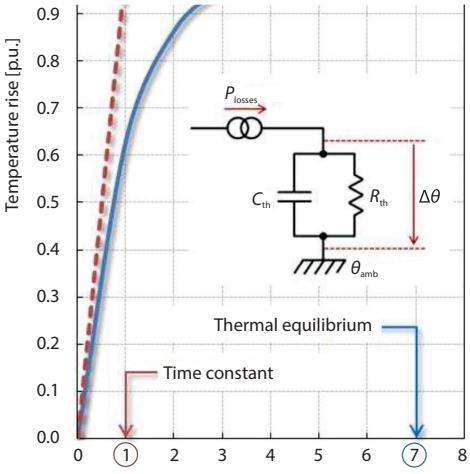

Figure 5. Temperature rise diagram of permanent magnet DC motor when the overload current is three times

The design weight of the EOD robot is 170-180 kg. Because the robot's wheel is designed with teeth, it can climb stairs with a slope of 40°. According to the design requirements, set the entire wheel mechanism's efficiency to 70%, then the wheel motor. The average torque that the robot needs to output on a staircase with a gradient of 40° is 1.853 Nm, and the peak torque that needs to be output when climbing the stairs is 4.69 Nm [9].

The parameters of the wheel motor are: power 250 W, rated torque 3000 rpm, rated torque 0.83 Nm, peak torque 7.0 Nm, rated voltage 24 V, rated current 13 A, insulation class F and motor size is 84 mm in diameter. Length 125 mm, armature size can be obtained from the manufacturer. When the robot is climbing stairs, the current overload multiple of the motor is only 2.23 times. Considering the safety factor, the motor's transient temperature rise is calculated as 2.5 times the overload current multiple [10].

The steady-state temperature rise of the wheel motor under overload current

For different overload currents, the steady-state temperature rise of the motor is also different. Substituting the motor parameters into eq. (10), the equation can be solved to obtain each part of the motor's temperature rise under different overload currents [11]. Figure 5 shows that the ambient temperature is 40 °C. The temperature rises law of a permanent magnet DC motor under

three times the overload current L_1, L_2 is 1/2 off L_a, L_j, and L_j is the end cover radius. It can be seen from the figure that even if the current of the wheel motor is overloaded three times, it can be seen from eq. (1). The life of the insulating material in the motor can also meet the life requirements of the EOD robot.

The transient temperature rise of wheel motor under overload current

Considering the steady-state temperature rise on flat ground, this article believes that the initial temperature of the motor at the beginning of the transient is 50-60 °C. According to the *Building Stair Modulus Coordination Standard* (GBJ101-86), when the staircase slope is 40°, The width of a single step can be 220 mm, the height is 180 mm, and each step does not exceed 18 steps. The robot's fastest speed on flat ground is 0.57 m/s, the average speed on the stairs with a slope of 40° is based on the motor. The current overload is calculated by 2.5 times, the fastest speed is 0.45 m/s, the shortest average time for the robot to climb 18 steps is about 11 seconds, but considering the time to enter and leave the steps, in the experiment, the robot takes 10-20 seconds This article specifies that the maximum temperature of the motor shell is 100 °C, and substitutes various parameters into eq. (13) for obtaining the time to reach the maximum temperature under different overload current multiples and different starting temperatures, see fig. 6.

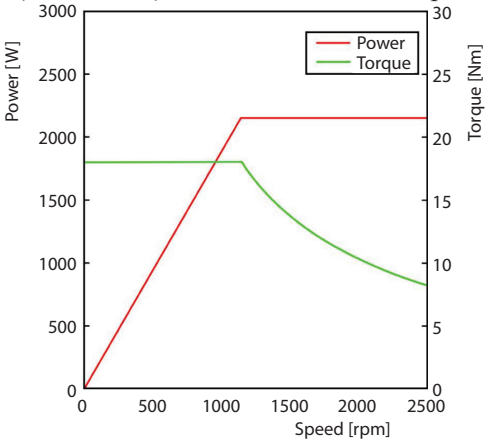

Figure 6. The time when the motor shell reaches the specified temperature varies with the initial temperature of the motor

It can be seen from the figure that when the overload current multiple is 2.5 times and the starting temperature of the motor is 60 °C, the time it takes for the motor to reach the maximum temperature of 100 °C is about 6.3 minute, which can fully meet the needs of the robot to climb stairs. Automatic adjustment detection circuit, the ability of magnification enables it to output a curve roughly consistent with the standard curve within its detection range so that the standard output curve can be used to determine the distance between the object and the sensitive skin.

Conclusions

The sensitive skin designed in this article can cover the robot's surface and rely on the infrared sensor and control circuit on the skin to perceive the external environment. It can greatly improve the robot's perception ability in an unknown environment and improve its autonomous workability. In signal processing, It adopts a modular method for processing and has the following characteristics.

- The modular structure of the skin is easy to re-modify to meet the actual needs of special robot arms and mobile robots.
- It improves the calculation speed of the signal to meet the need for real-time processing.
- Reduce the size of the control circuit to make it easy to paste on the surface of the robot.

Acknowledgment

This study was co-supported by the Hebei Province Innovation Capability Enhancement Project (Grant: 20555404K) and Funded by Science and Technology Project of Hebei Education Department (Grant: Z2019052).

References

[1] Clayton, G. M., Mechatronics for Humanitarian Explosive Ordnance Disposal in Cambodia, *Mechanical Engineering*, *140* (2018), Suppl., 9, pp. S4-S10
[2] Jin, M., *et al*., Research Trends on Disaster Response Robots, *Journal of the Korean Society for Precision Engineering*, *36* (2019), 4, pp. 331-337
[3] Li, G., *et al*., A Novel Feature Extraction Method for Machine Learning Based on Surface Electromyography from Healthy Brain, *Neural Computing and Applications*, *31* (2019), 12, pp. 9013-9022
[4] Wu, S., Construction of Visual 3-D Fabric Reinforced Composite Thermal Perfomance Prediction System, *Thermal Science*, *23* (2019), 5, pp. 2857-2865
[5] Luo, B., *et al*., Decomposition Algorithm for Depth Image of Human Health Posture Based on Brain Health, *Neural Computing and Applications*, *32* (2020), 10, pp. 6327-6342
[6] Li, J., *et al*., Hand Motions Recognition Based on sEMG Non-Linear Feature and Time Domain Feature Fusion, *International Journal of Innovative Computing and Applications*, *10* (2019), 1, pp. 43-50
[7] Cheng, W., *et al*., Jointly Network: A Network Based on CNN and RBM for Gesture Recognition, *Neural Computing and Applications*, *231* (2019), 1, pp. 309-323
[8] Guzman, R., *et al*., Development of a Modular Chemical, Biological, Radiological, and Nuclear Robot for Intervention, Sampling, and Situation Awareness, *Journal of Field Robotics*, *33* (2016), 7, pp. 931-945
[9] Crampton, W. G., Electroreception, Electrogenesis and Electric Signal Evolution, *Journal of Fish Biology*, *95* (2015), 1, pp. 92-134
[10] Schacht-Rodríguez, R., *et al*., Path Planning Generation Algorithm for a Class of UAV Multirotor Based on State of Health of Lithium Polymer Battery, *Journal of Intelligent & Robotic Systems*, *91* (2018), 1, pp. 115-131
[11] Wu, S., Construction of Visual 3-D Fabric Reinforced Composite Thermal Perfomance Prediction System, *Thermal Science*, *23* (2019), 5, pp. 2857-2865

Paper submitted: November 21, 2020
Paper revised: January 4, 2021
Paper accepted: January 20, 2021

© 2021 Society of Thermal Engineers of Serbia
Published by the Vinča Institute of Nuclear Sciences, Belgrade, Serbia.
This is an open access article distributed under the CC BY-NC-ND 4.0 terms and conditions